Single-Step PEDOT Deposition by oCVD for ITO-Free Deep Blue OLEDs

Abderrahime Sekkat, Houssein El Housseiny, Eleni Poupaki, Benjamin Breig, Diane Samélor, Jérôme Esvan, Olivier Marsan, Cédric Charvillat, Alessandro Pugliara, Nicolas Caussé, et al.

Single-Step PEDOT deposition by oCVD for ITO-free deep blue OLEDs

Journal:	*ACS Applied Polymer Materials*
Manuscript ID	ap-2023-02019u.R1
Manuscript Type:	Article
Date Submitted by the Author:	04-Oct-2023
Complete List of Authors:	Sekkat, Abderrahime; LGC, Université de Toulouse, Toulouse INP, CNRS, Toulouse France Houssein, El Housseiny ; LAPLACE Poupaki, Eleni; LGC Breig, Benjamin ; LGC Samélor, Diane; Universite Federale Toulouse Midi-Pyrenees, INPT-CIRIMAT Esvan, Jérôme; CIRIMAT, CNRS-UPS-INPT, ENSIACET Marsan, Olivier; CIRIMAT Charvillat, Cedric; CIRIMAT Pugliara, Alessandro; CIRIMAT Caussé, Nicolas; CIRIMAT Vergnes, Hugues; LGC Ternisien, Marc; LAPLACE Renaud, Cedric; Universite Toulouse III Paul Sabatier, Zissis, Georges; LAPLACE Caussat, Brigitte; Laboratoire de Génie Chimique - UMR CNRS 5503,

Single-Step PEDOT deposition by oCVD for ITO-free deep blue OLEDs

Abderrahime Sekkat[1,], Houssein El Housseiny[2], Eleni Poupaki[1], Benjamin Breig[1], Diane Samélor[3], Jérôme Esvan[3], Olivier Marsan[3], Cédric Charvillat[3], Alessandro Pugliara[3,4], Nicolas Caussé[3], Hugues Vergnes[1], Marc Ternisien[2], Cédric Renaud[2], Georges Zissis[2], Brigitte Caussat[1,*]*

[1] LGC, Université de Toulouse, Toulouse INP, CNRS, Toulouse France.

[2] LAPLACE, Université de Toulouse, Toulouse INP, CNRS, UPS, Toulouse France.

[3] CIRIMAT, Université de Toulouse, Toulouse INP, CNRS, Toulouse France.

[4] Centre de MicroCaractérisation Raimond Castaing, Université de Toulouse, Toulouse INP, INSA Toulouse, CNRS, Toulouse, France.

KEYWORDS: oCVD, PEDOT, OLED, ITO-free, solvent-free TCE.

ABSTRACT

Organic light-emitting diodes (OLEDs) are emerging technologies for potential lighting and display applications. Transparent conductive electrodes (TCEs) play a crucial role in enabling the functionality and increased performance of these particular devices. Despite its widespread use, indium tin oxide (ITO) thin films have several significant drawbacks, including material scarcity, high costs associated with both materials and fabrication processes, and limited flexibility. To address these issues, we thoroughly investigate the deposition of Poly (3,4-ethylenedioxythiophene) (PEDOT) thin films, as a promising alternative to ITO, using a single-step and dry method named oxidative chemical vapor deposition (oCVD). The impact of increasing the substrate temperature from 110 ˚C to 190 ˚C on the film's structure and properties was revealed with an increase in the film conductivity to over 1600 S/cm at 170 ˚C and a total transmittance of 97% in the visible range. This increase was attributed to a change in the molecular structure of the conjugated polymer from benzoid to quinoid, as revealed by Raman and FTIR measurements. The XPS results demonstrated an increase in doping ratio with Cl-containing species and a reduction of impurities. GIXRD, HR-TEM, and AFM measurements indicated a smooth surface and a highly face-on orientation for all temperatures. The optimized TCE layers

were successfully integrated into deep blue OLED devices emitting at 436 nm with a stable color Commission Internationale de l'Energie (CIE) coordinates of (0.15, 0.08) under variation of the applied current. The performance (72.1 Cd/m² and 0.86 W/Sr.m² at 10 mA.cm^{-2}) and an external quantum efficiency (EQE) of 1.04% were achieved. These results are quite promising, as OLEDs based on PEDOT as a TCE have demonstrated slightly better output performance in terms of luminance and radiance, with an increase in EQE by the factor of 1.7, compared to the reference device based on ITO.

1. INTRODUCTION

Organic light-emitting diodes (OLEDs) have led the way for display and lighting applications with their superior performance in terms of color gamut and luminance efficiency[1–4]. This technology is widely used in everyday applications such as smartphones and digital cameras and is a potential candidate for the Internet of Things IoT, e.g. temperature and humidity meters based on OLED displays[5–7]. Nevertheless, several challenges still need to be overcome to achieve even better devices with great output performances. One such challenge is to enhance the device architecture by reducing the number of layers that can lead to a high probability of photon trapping. Another highly significant bottleneck is the replacement of indium tin oxide (ITO) thin films as electrodes for this particular device. In fact, the scarcity and expensive cost of the latter require to develop alternative cost-effective materials[8]. Further, the brittleness of this particular material and its manufacturing process make it less appealing for further development. Besides, polystyrene

sulfonate (PSS)-doped Poly (3,4-ethylenedioxythiophene) PEDOT is commonly used in OLEDs to promote hole injection and thus improve light coupling and device efficiency[9]. This has been demonstrated in several works in which solution-processed PEDOT:PSS layers (post-treated with benzoid acid[10] and acetone[11]) were incorporated into OLEDs revealing an enhanced luminance[11]. Although PEDOT:PSS helps to improve the performance of OLEDs, it still depicts several drawbacks in terms of anisotropic charge injection, hygroscopicity, and acidity, which thus leads to device degradation and limits operational stability[12]. In addition, PSS counter ion restrict the electrical conductivity of the PEDOT due to its insulating nature, resulting in undesirable changes on various properties such as work function and band alignement[13]. Although PEDOT:PSS is currently used as hole injection layer (HIL) within ITO based OLEDs[14,15], all the above, mainly its poor electrical conductivity, restraints its successful integration in OLED devices as an efficient ITO free TCE.

To this end, pristine PEDOT represents an excellent alternative to transparent conducting oxides (TCOs) due to its high optical transparency, high electrical conductivity, and promising mechanical flexibility. In fact, several routes are known to produce PEDOT thin films, all belonging to liquid-based methods from spin coating, particularly for PEDOT:PSS[16–18], to chemical polymerization[19,20], electropolymerisation[21,22], and even vapor phase polymerization (VPP) which involves a first liquid step[23,24]. Another original approach, known as the oxidative chemical vapor deposition (oCVD) process, was introduced by the Gleason group[25,26]. It is a dry and one-step technique that allows for the precise deposition of high-quality PEDOT films at low temperatures (<200 °C) and under reduced pressure (<200 Pa), allowing conformal coatings on complex or thermosensitive substrates while avoiding solvent-substrate issues. The conjugated polymer is then synthesized through gas phase injection of 3,4-ethylene dioxythiophene (EDOT)

as monomer and one oxidant. Further, the solid oxidant iron trichloride ($FeCl_3$) was the first and most common one to be studied[27,28,37–41,29–36], while in recent years, liquid oxidants, namely (3-thiophene acetic acid (TAA)[42], vanadium oxytrichloride ($VOCl_3$)[43–45], sulfurice acide (H_2SO_4)[46], bromine (Br_2)[27], molybdenum(V) chloride ($MoCl_5$)[47], copper(II) chloride ($CuCl_2$)[48], and antimony pentachloride ($SbCl_5$)[43,49–51], have replaced it with the aim of optimizing the performance of PEDOT and avoiding sublimation drawbacks. Among these candidates, $SbCl_5$ has recently emerged as one of the most commonly used precursors, due to its low toxicity, high volatility, and cost-effectiveness, compared to other compounds such as molybdenum(V) chloride ($MoCl_5$) or vanadium oxytrichloride ($VOCl_3$)[49]. This enables the efficient deposition of highly conductive films through oCVD, making it a robust process for successful integration into several applications, as evidenced by the few publications using this particular precursor[43,49–51].

The most commonly accepted mechanism for PEDOT deposition through the oCVD process involves the oxidation of monomers to form radical cations, the dimerization of cation radicals, the deprotonation of dimers to obtain conjugation and their oxidation within the step-growth polymerization process forming the growing polymer chain. Some of the positively charged heterocyclic rings are stabilized by the presence of counterions, known as dopants, e.g. Cl^- and/or $SbCl_6^-$ [49]. So, the mixture of the oxidant and monomer vapors in suitable processing conditions allows polymerization, doping, and thin film formation to occur simultaneously, providing two polymeric molecular structures, namely benzoid or quinoid[52,53]. The quinoid conformation displays higher conductivity due to enhanced charge delocalization and the presence of alternating double bonds, which promote stronger intra-chain coupling and thereby improve electrical conductivity. Still, the overall electrical film conductivity is also impacted through inter-chain coupling even though it is considered weaker than intra-chain one[49,53]. This is mainly due to

the low charge carrier mobility through the π-π inter-chain. To enhance the charge mobility at the inter-chain coupling, it is essential to reduce the π-π distance, which helps prevent charge localization caused by defects and amorphous regions[53]. In fact, PEDOT is formed of a complex micro-, and nano-structure of ordered crystalline regions embedded in an amorphous matrix, which must be controlled to avoid charge localization. Besides, the crystallographic orientation of the crystalline regions can greatly impact the film conductivity through creating an anisotropy in charge transport that is either parallel or perpendicular to the conjugation direction. Commonly, the PEDOT orientation is based on the face-on orientation where the stacking of π-π interchain is parallel to the substrate's plane, whereas in the edge-on orientation, the stacking is perpendicular to the substrate's plane. A mixture of both orientations leads to a high-angle grain boundary, which creates defects and increases the energy barriers for intercrystallite charge transfer, thereby reducing electrical conductivity[53]. For these reasons, it is important to maintain a low level of heterogeneous orientations to prevent recombination keeping whether a highly face-on or edge-on orientation (no orientation anisotropy and better percolation pathway).

In the present study, we have thoroughly investigated the deposition of PEDOT thin films by oCVD using EDOT as a monomer and $SbCl_5$ as an oxidant. Furthermore, following previous works of our group performed in a cold wall reactor[40,50], the PEDOT deposition was carried out using a hot-wall reactor with the aim of improving film uniformity over a large surface area. Thus, the aim of this study is to investigate the influence of the substrate temperature, ranging from 110 °C to 190 °C, on the structure, morphology, and properties of PEDOT thin films deposited on glass and silicon substrates. This is done towards enhancing the film properties and facilitate the efficient integration into blue OLED devices as an alternative to ITO. Thus, a proper approach, such as oCVD, allows to generate solvent-free PEDOT thin films under reduced pressure and temperature

while inducing doping at once. To the best of our knowledge, no reported work has shown improved OLED performance using electrodes based solely on oCVD-PEDOT replacing ITO. These findings demonstrate the significant potential of oCVD-PEDOT layers in OLED devices, paving the way for the development of next-generation organic optoelectronics.

2. METHODS

2.1. Film deposition

oCVD experiments are performed in a custom-built horizontal tubular hot-wall borosilicate glass reactor of 4.9 cm in diameter and 32 cm long, as schematically presented in Supplementary Figure S1. PEDOT films were deposited on borosilicate glass substrates (3.4 cm x 2.2 cm) and Si (100) wafers cut in centimetric coupons, placed on a horizontal rectangular platen as illustrated in **Figure 1a**. The reactor is equipped with a heating jacket connected to a PID controller to monitor homogeneous wall temperatures and with heating ribbons at its two extremities. A thermal calibration pre-deposition step under pure nitrogen allowed to obtained an isothermal substrate temperature along the reactor length at 110, 130, 150, 170, and 190 °C. The total pressure is controlled by a system composed of a XDS 10 scroll dry pump (Boc Edwards), a gate valve, and a Baratron pressure gauge. The total pressure is fixed at 42 Pa and the deposition time has been varied from 2 to 10 min, targeting film thicknesses in the range 5 to 50 nm. PEDOT films were produced from monomeric 3,4-ethylenedioxythiophene (EDOT, 97%, Sigma-Aldrich) and $SbCl_5$ (99.99%, Sigma-Aldrich). The liquid reactants, $SbCl_5$ and EDOT were evaporated from glass bubblers and placed in a thermally-regulated oven at 90 °C. The bubblers were loaded in a glove box under argon atmosphere. All gas lines between the bubblers and the reactor inlets were heated at 100 °C to avoid condensation of the gas phase. A flow of 20 standard centimeters per minute (sccm) of nitrogen (99.999%, Messer) was also sent into the reactor during the depositions in order

to dilute the reactants. The samples were first cleaned with water, acetone, and isopropanol in an ultrasonic bath for 5 min each, then dried with argon followed by a UV-Ozone plasma cleaning for 10 min. Before and after each experiment, the mass difference of the $SbCl_5$ and EDOT bubblers was systematically measured using a KERN ABS 320-4 N balance with a precision of 0.1 mg. This procedure allowed us to ascertain the flow rates of the vaporized EDOT and $SbCl_5$, thus the inlet molar $SbCl_5$ on EDOT ratio of 1:0.84.

2.2. Characterization techniques

Film thickness was measured with cross-section Focused ion beam (FIB) - Scanning electron microscopy (SEM) (THERMO FISHER, Helios NanoLab 600i) and through atomic force microscopy (AFM) after inducing a step height. AFM maps were obtained using a dimension ICON (BRUKER). Further, a thin foil was prepared using the focused ion beam-lift out technique in FIB-SEM to allow Transmission electron microscopy (TEM) analysis (imaging: High resolution TEM (HR-TEM) and Scanning TEM - High angular annular dark field (STEM-HAADF); and chemical composition mapping: Scanning TEM - Energy dispersive X-ray spectroscopy (STEM-EDX)). TEM imaging was performed using electron microscope JEOL JEM 2100 F operated at 200 kV equipped with an Energy dispersive X-ray (EDX) analyzer (Oxford instrument Ultim®Max 100 mm^2). The film was analyzed using transmission Fourier transform infrared spectrometry (FTIR), with Frontier PerkinElmer spectrometer. Each spectrum was acquired with 16 scans at 4 cm^{-1} resolutions. The baseline has been performed for each spectrum with Omnic 9.1 software. Optical transmittance of films deposited on purpose on glass substrates (Deckglaser 0101062) was measured using an Agilent Cary 5000 UV-Vis spectrometer within the range of 300-800 nm. A 600 nm/min scan rate with 2 nm spectral bandwidth (SBW) was applied. The film sheet resistance Rs was measured on the wafer substrates with a Signatone S-302-4 four-point

probe station. A current ranging from 1000 nA to 10000 nA was applied with a Keithley 6220 instrument, and the corresponding voltage was read on a Keithley 2182A one. Raman analyzes on films were carried out using a confocal Raman Labram HR 800 Horiba Yvon Jobin microscope. The samples were exposed to continuous laser radiation supplied by an argon laser at 532 nm with a power of 0.8 mW. Attenuation filters were used to avoid any degradation of the materials lowering the laser power by ten. Each spectrum was acquired with a 30 second time and 3 accumulations. Data processing was performed using Labspec 6 software. Grazing incidence X-ray diffraction (GIXRD) data was achieved with a D8-Bruker Advance instrument using a Cu Ka (1.5418 A˚) X-ray tube operating at 40 kV and 40 mA, a Göbel mirror and a solid-state Lynxeye detector. The measurements are investigated in the range of $2\Theta = 5\text{-}35°$ with an angle of incidence of 2° with 10 s steps. For the X-ray photoelectron spectroscopy (XPS) analyses, the photoelectron emission spectra were recorded using a monochromatised Al Kalpha ($h\nu = 1486.6$ eV) source on a ThermoScientific K-Alpha system. The X-ray spot size was about 400 µm. The pass energy was fixed at 30 eV with a step of 0.1 eV for core levels and 160 eV for surveys (step 1eV). The spectrometer energy calibration was done using the Au $4f_{7/2}$ (83.9 ± 0.1 eV) and Cu $2p_{3/2}$ (932.8 ± 0.1 eV) photoelectron lines. XPS spectra were recorded in direct mode N(Ec) and the background signal was removed using the Shirley method. The flood gun was used to neutralize charge effects on the top surface. The water contact angle of the PEDOT thin film was measured using the sessile drop method (DIGIDROP, GBX) on a silicon substrate coated with PEDOT. Water droplets were deposited onto the sample surface using a micro syringe fixed on the DIGIDROP GBX equipment.

2.3. Device Fabrication and testing

OLED device structure being considered in this work consisted of TCE as anode/ N,N′-Di(1- naphthyl)-N,N′-diphenyl-(1,1′-biphenyl)4,4′diamine (NPD) as both hole transporting layer

(HTL) and emissive layer (EML)/ 2,2',2''-(1,3,5-Benzinetriyl)-tris1-phenyl-1-H-benzimidazole (TPBi) as both electron transport layer (ETL) and exciton blocking layer (EBL)/ Calcium (Ca, 80 nm) as cathode. Two types of TCE based OLED were fabricated. PEDOT based TCE were coated on glass substrate by using oCVD process as described in previous section. ITO based TCE consist of 100 nm of ITO coated glass substrates from Kintec with a sheet resistivity 15Ω/square. The ITO glass substrates were cleaned sequentially with deionized water, acetone, ethanol, isopropanol and treated with UV ozone right before organic deposition. A thickness of 95 nm for NPD and 35 nm for TPBi was chosen in order to confine exciton formation within NPD layer close to the interface with TPBi. This OLED structure led to deep blue emission (at 436 nm) originated from NPD emission. All these materials were purchased from Kintec. The organic materials and the cathode were deposited by thermal evaporation in a multiple-source chamber under high vacuum ($<10^{-5}$ mbar). An *in situ* quartz crystal microbalance (QCM) was used to monitor the thickness of the layers. The active area of the device was 18.28 mm^2. Characterizations of the OLEDs were obtained under inert atmosphere. Electrical characterization (I-V) of devices was performed using a Current-Voltage source (Keithley). The electroluminescence spectra, the luminance and the Commission Internationale de l'Energie CIE coordinates were measured by using a spectroradiometer (JETI SpecBos 1201).

3. RESULTS AND DISCUSSION

Figure 1b details the PEDOT deposition rate R_d evolution for the glass substrates along the reactor length (samples B, D, E and F) for the various substrate temperature T_{sub} tested at 110, 130, 150, 170 and 190 °C. The corresponding variations of the PEDOT film thicknesses are provided in Supplementary Figure S2. It appears first that the average R_d on the whole substrates of a given experiment tends to decrease when T_{sub} increases, as already found by other authors[49,50].

It indeed varies from 0.24 ± 0.06 nm/s at 110°C to one order of magnitude lower values for samples deposited at 190 °C. This trend could be explained by the fact that for this range of operating conditions, the PEDOT deposition process is most likely limited by the $SbCl_5$ availability near the substrate surface[50]. Higher temperatures reduce vapor-to-surface adsorption and therefore limit the amount of oxidant available for surface reaction[50]. The range of R_d obtained is comparable to those of previous works for close deposition conditions[51]. Moreover, the uniformity in R_d and then in thickness along the reactor length and even on each substrate markedly increases with T_{sub}. Indeed at 110 °C, R_d decreases from 0.35 nm/s for sample B to 0.08 nm/s for sample F (corresponding to thicknesses between 43 and 10 nm). The thickness variation is less pronounced at 130°C (32 to 15 nm) and becomes negligible for samples D to F at 170 °C (thickness close to 4.7 ± 1.4 nm) and 190 °C (thickness close to 1.8 ± 1 nm), leading to a 10 cm long uniform region. This behavior could be due to the fact that as the average R_d is higher at low temperature, the reactants consumption along the reactor length is higher too, leading to a more marked depletion in precursors and then to a mass transport limited process at 110 °C and 130 °C. Thanks in particular to the low total pressure imposed, the process is kinetically limited at the other temperatures, which is very favorable to uniformly coat large substrates.

For these same samples, the average film electrical conductivity for the whole substrates of a same experiment shows a gradual increase with T_{sub} from 110 °C (~80±20 S/cm) to 170 °C (~1600±50 S/cm) (**Figure 1c**), as was already observed by other studies[43,50]. At 190 °C, the average conductivity for samples D to F drops markedly to values close to 144 ± 41 S/cm, while that of sample B located near the reactor entrance remains at 1262 ± 380 S/cm. This is probably due to the fact that at T_{sub} of 190 °C, the gaseous $SbCl_5$ is decomposed in non-reactive by-products, the main one being the volatile $SbCl_3$ species, knowing that the $SbCl_5$ decomposition temperature is

equal to 180 °C[49,54]. This decomposition is probably moderate for sample B as it is the closest one from the inlet and much more marked after 7-8 cm from the entrance for the other samples. Previous works using $SbCl_5$ oxidant were performed at temperatures below 180 °C, which explains why this phenomenon has not been observed previously[43,49–51]. The conductivities are quite uniform along the reactor length for all the other T_{sub}, except for sample B at 170 °C which presents a 25% lower conductivity in comparison with samples D to F. This discrepancy could be another time due to the fact that sample B is the closest one from the reactor inlet and that the gaseous reactants could have not yet reached the target temperature of 170 °C in this zone. Besides, the average square resistance of the different samples is added to Supplementary Table S1. Some of these values lie within the suitable range required for the integration of such layers in OLED devices.

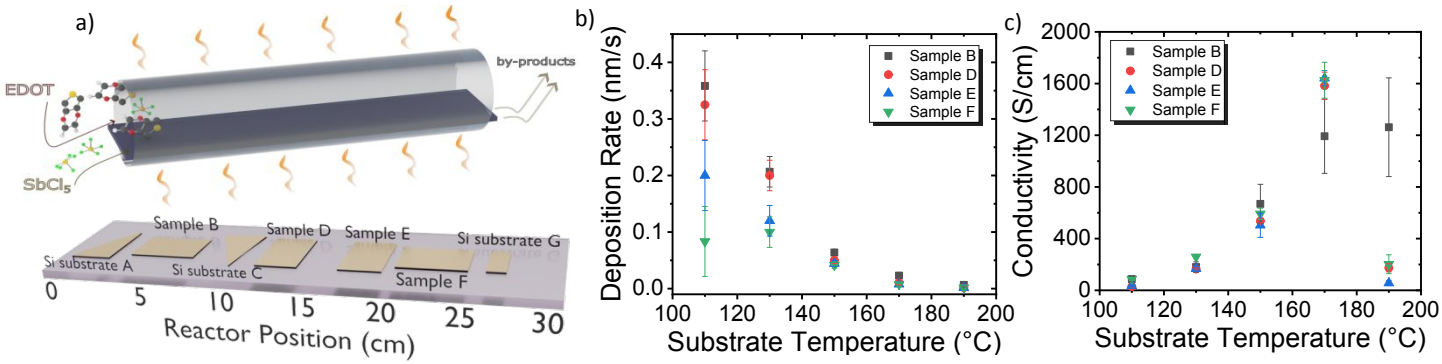

Figure 1. (a). Illustration of the oCVD reactor used for the deposition of PEDOT thin films with the schematic view of the 30 cm platen on which seven samples are placed, samples A, C and G being silicon substrates and samples B, D, E and F being borosilicate glass substrates. **(b).** deposition rate, and **(c).** electrical conductivity variation, of PEDOT thin films grown on glass substrates at different temperatures. Error bars represent min/max values obtained for each point from six different measurements throughout the entire sample.

Furthermore, as illustrated in Supplementary Figure S3, it can be observed that the film transmittance at 556 nm shows a slight increase, ranging from approximately 85% to 98%, as the deposition temperature increases. These values are highly favorable for the integration of such TCEs in OLED devices. This trend is directly correlated to the variations in film thickness, as depicted in Supplementary Figure S2. In the following part, only two substrates for each experiment, sample A (silicon) and sample B (glass), were analyzed. The substrate selection was based on the compatibility of each substrate with the film characterization method.

Further, the successful polymerization of the EDOT monomer units was confirmed by FTIR due to the presence of the expected vibration modes. Supplementary Table S2 depicts all the identified frequencies from the FTIR measurement. Specifically, the characteristic peaks of PEDOT are observed in the vibrational modes of the thiophene ring at 819 cm^{-1} and 944 cm^{-1}, as well as the ethylenedioxy rings at 1061 cm^{-1}, 1113 cm^{-1}, and 1154 cm^{-1} [43,49]. Furthermore, the absence of peaks associated with C_{α}-H stretching at 1310 cm^{-1} and 754 cm^{-1} confirms the successful polymerization of the PEDOT chain[49]. Besides, the FTIR measurements show the presence of both PEDOT structures, benzoid at 1448 cm^{-1} and quinoid at 1560 cm^{-1} positions (**Figure 2a**), which are associated with the asymmetric stretching of the C=C bond and C-C inter-ring range respectively. Moreover, **Figure 2b** illustrates the evolution with T_{sub} of the under-curve surface integral of benzoid and quinoid structures (presented in **Figure 2c**), along with the quinoid/benzoid ratio. As the T_{sub} increases, the ratio of quinoid to benzoid structures tends to rise from 0.5 towards 1.3, resulting in a higher proportion of quinoids. This trend aligns with the previously observed increase in electrical conductivity exhibited by the PEDOT thin films. Furthermore, **Figure 2d** represents the Raman spectra of deposited PEDOT films of sample A at different T_{sub} within the range of 1350 cm^{-1} to 1550 cm^{-1}. The peaks observed are similar to those

previously reported for the oCVD synthesis of PEDOT with the same liquid oxidant ($SbCl_5$)[43,49]. The 1368 cm^{-1} peak position shows the presence of C_β -C_β stretching vibration, while the symmetric and asymmetric vibrations of C_α=C_β are detected at 1439 cm^{-1} and 1505 cm^{-1} peaks, respectively, confirming PEDOT formation in all samples[49]. Further, as T_{sub} increases, the broadening of the C_α=C_β asymmetric peaks is depicted. This is induced through an additional band on the high wave number (1445 cm^{-1}), whose intensity increases with T_{sub} and which suggests the emergence of more quinoid structures. This observation is consistent with the FTIR measurements and previous reports in the literature[43,49].

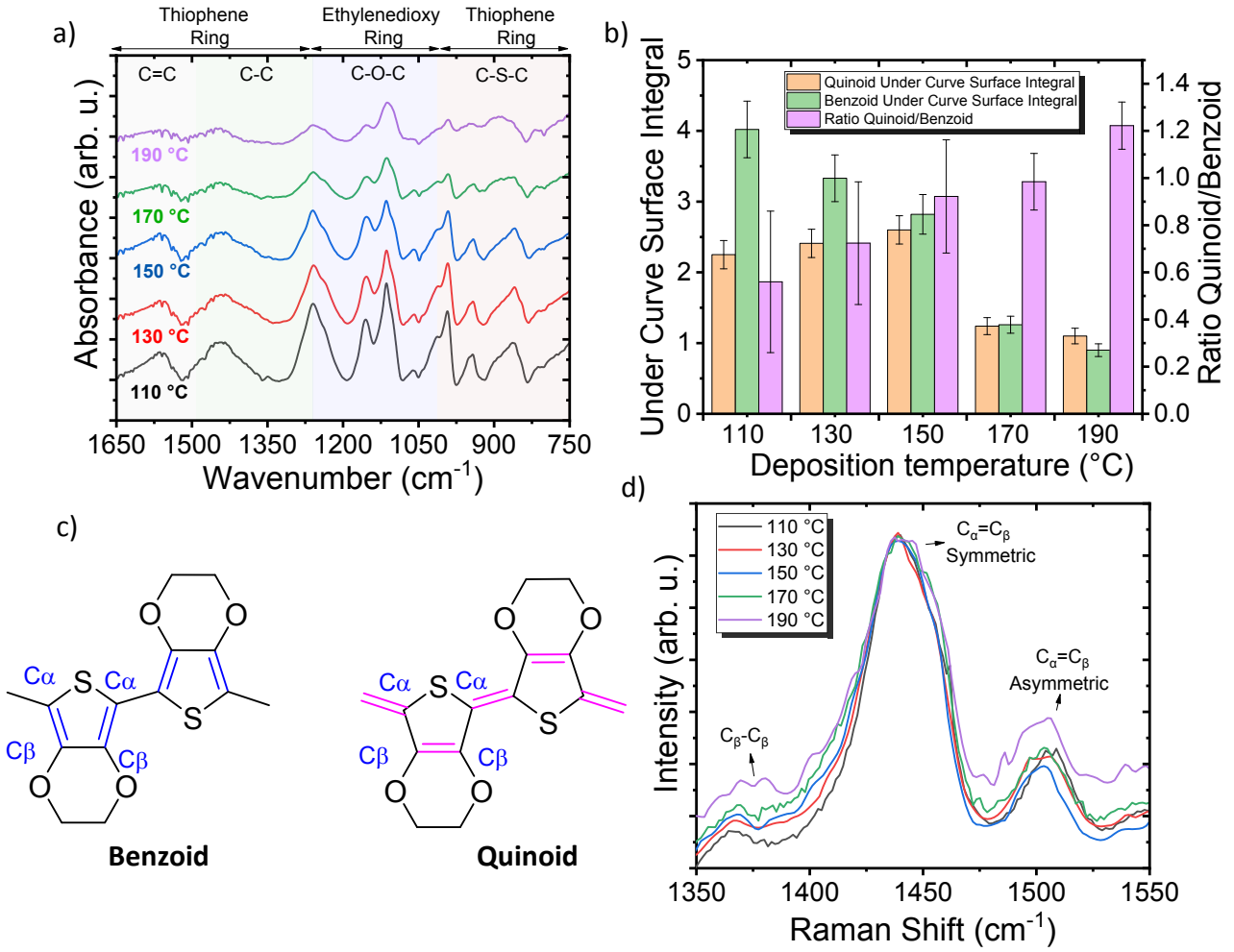

Figure 2. (a). FTIR spectra of PEDOT thin films deposited on silicon sample A at different substrate temperatures, **(b).** Under curve surface integration of the benzoid and quinoid forms of PEDOT thin films at different substrate temperatures along with the quinoid/benzoid ratio, **(c).** Molecular structure of the benzoid and quinoid forms of PEDOT, and **(d).** Raman spectra of PEDOT thin films deposited on silicon Sample A at different substrate temperatures.

Additionally, XPS measurements were performed on sample B without any etching process at two different T_{sub} (110 °C and 150 °C) to decouple the influence of doping and impurities on the film properties (**Figure 3**). The responses of Cl 2p, S 2p, O 1s and Sb 3d were studied to

determine the contributions of these elements, as detailed in Supplementary Table S3. Three chemical environments were identified within the Cl 2p spectrum, whether ionic Cl, Cl-Sb, and Cl-C species. The samples deposited at these temperatures contain a total Cl 2p of 1.45±0.5 at.%, out of which 0.3 at.% is attributed to the Cl-Sb bounds (**Figure 3a**). This value (1.45±0.5 at.%) is slightly comparable to the 2.4 at.% of Cl 2p found in PEDOT thin films reported by *Kaviani et al*., prepared using the same precursors. The main distinction is that *Kaviani et al.* enhanced the electrical conductivity of their films by subjecting them to post-deposition HCl cleaning. Initially, their as-deposited samples depicted a higher Cl content of 13.9 at.%, which decreased to 2.4 at.% after the cleaning step. The observed reduction was attributed to the decrease of ionic chlorine species ($SbCl_x$), resulting in the predominance of Cl^- dopants during the HCl post-treatment[43]. In our case, it appears that a lower Cl value (1.45±0.5 at.%) was obtained without requiring any additional treatment step, which could indicate most suited deposition conditions in terms of $SbCl_5$ on EDOT ratio. This confirms that the doping primarily occurred through Cl^- ions, as the Cl-Sb content in our case is quite low with respect to the values reported within the literature[43,49,52]. Furthermore, our analysis conclusively showed the absence of any unreacted, trapped $SbCl_5$ precursor, which could potentially introduce impurities into our films. These findings provide confirmation that the operating conditions, particularly in terms of the $SbCl_5$ to EDOT ratio, were appropriately selected for our study.

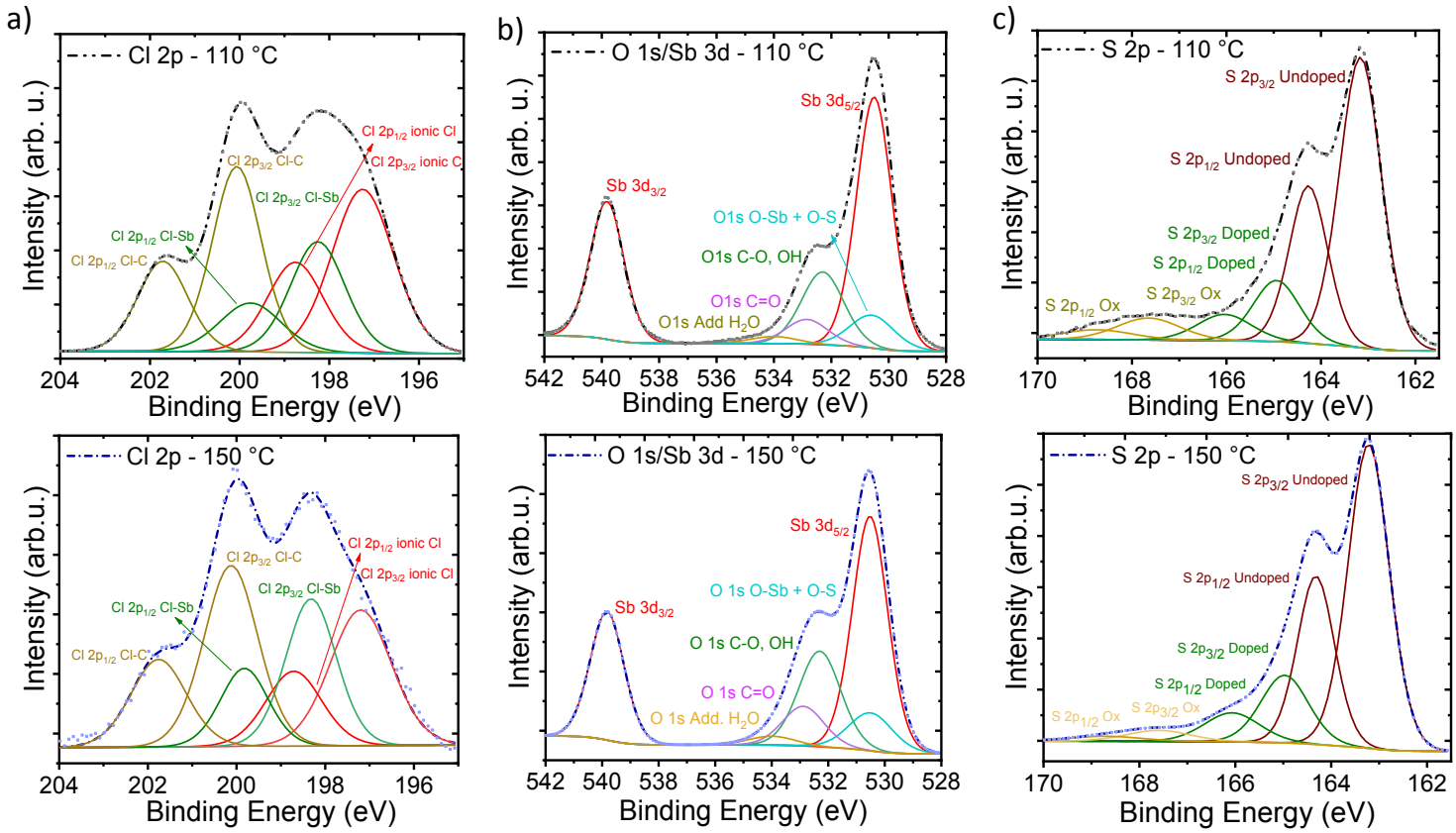

Figure 3. Chemical environments on the XPS spectra of PEDOT thin films deposited on sample B at 110 °C and 150 °C, **(a).** Cl 2p, **(b).** O 1s and Sb 3d, and **(c).** S 2p.

Furthermore, the O 1s core level exhibits four distinct peaks associated with O-Sb + O-S, C-O/OH, C=O, and adsorbed water, along with characteristic antimony peaks (**Figure 3b**). The decrease of the Sb-Cl content from 3.1 at.% at 110 °C to 2.1 at.% at 150 °C indicates a reduction of the ionic configurations of the precursor ($SbCl_x$) that could potentially act as dopants within the films. Additionally, the percentage of O-Sb + O-S decreases from 6.9 at.% at 110 °C to 5.9 at.% at 150 °C, suggesting a reduction in sulfur oxidation. This aligns with the S 2p core level analysis (**Figure 3c**), which indicates a decrease in the amount of the oxidized sulfur from 0.6 at.% at 110 °C to 0.3 at.% at 150 °C. This observation is consistent with previous research indicating that

sulfur oxidation usually occurs from 130 °C[55]. Moreover, the S 2p analysis revealed a slight increase in the doped to undoped S ratio from 0.24 at 110 °C to 0.27 at 150 °C, which could partially explain the enhanced film conductivity. The obtained ratio is consistent with previous work that used similar precursors[43]. In fact, most studies report that the oxidation level of heavily doped PEDOT is typically 33%, corresponding to one charge per three monomer units[53,56,57]. Furthermore, the C 1s peak values were found to be comparable at all temperatures, as shown in Supplementary Figure S4, which aligns well with the reported findings in the literature[43,49]. The predominance of C-C bounds in the C 1s peak can be attributed to the presence of the PEDOT backbone. On the other hand, the presence of C-O bounds is likely a result of the specific arrangement or conformation of the PEDOT structure. It is important to note that the C-O signal might also be influenced by potential CO_2 contamination from the atmosphere[43].

In addition, PEDOT films may exhibit different crystalline orientations, with two prevalent ones being face-on (020) and edge-on (100), as shown in **Figures 4a&b** respectively[53]. **Figure 4c** presents the Grazing incidence X-ray diffraction (GIXRD) patterns of the PEDOT thin films deposited on sample B at 110, 150, and 190 °C. The patterns depict two crystalline planes (100) and (020) for all the three different temperatures[33,53]. The intensities are similar across the different samples, indicating a dominant contribution of the face-on orientation with a slight (<10%) contribution of the edge-on orientation, as shown in **Figure 4d**. It can then be concluded that in our case, the impact of the crystallographic orientation on the film conductivity across the evolution of T_{sub} is not very significant, as the film predominantly exhibits a highly face-on orientation over all the samples.

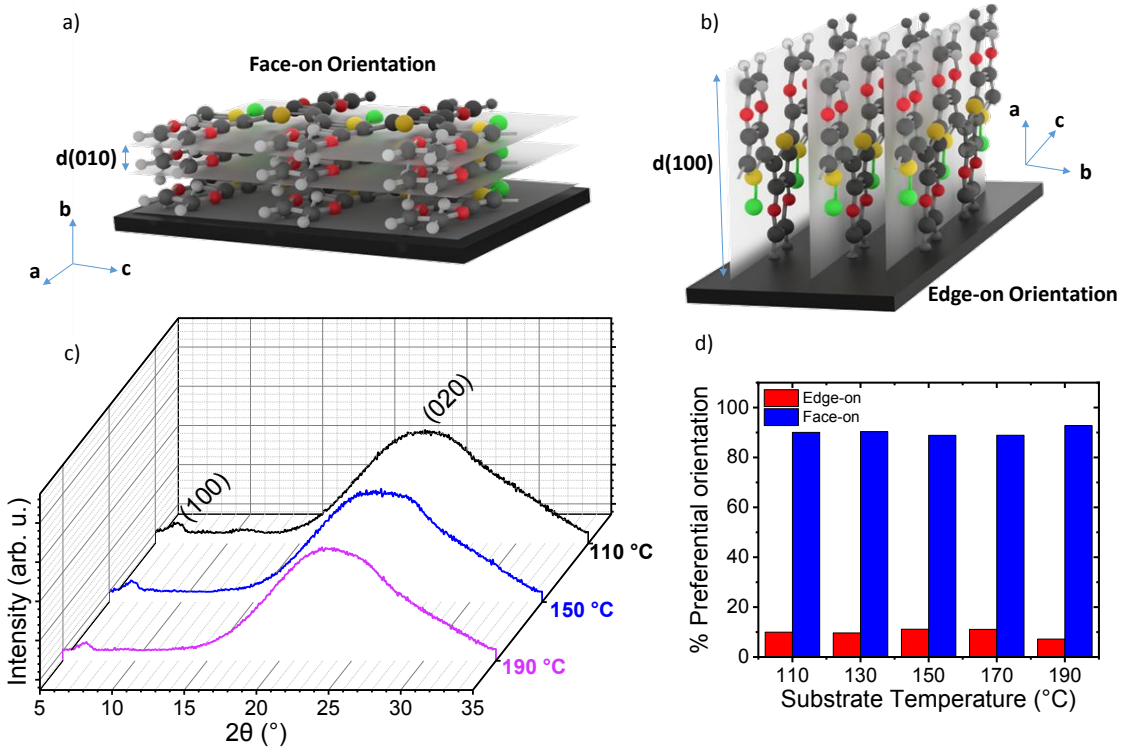

Figure 4. Illustration of **(a).** the face-on orientation and **(b).** the edge-on orientation, **(c).** GIXRD patterns of PEDOT thin films deposited on glass substrate B at 110, 150 and 190 °C, **(d).** Ratios between the face-on and edge-on orientations in the PEDOT thin films for the various substrate temperatures.

Although this configuration may lead to less recombination and improved charge transfer within the layer, intra-chain transport within the conjugated backbone surpasses inter-chain transport in terms of charge carrier mobility, as previously mentioned. In fact, it is likely that the increase in the PEDOT conductivity with increase of T_{sub} in our processing conditions is mainly due to an improvement of the intra-chain transport associated with the doping level and molecular structure. In addition, previous few studies investigating the deposition of PEDOT thin films using the same reagents have found no evidence of crystallinity in the PEDOT film, likely due to the low deposition temperatures and/or different process conditions[43,50]. Conversely, *Gharahcheshmeh et*

al.[49] reported on semi-crystalline PEDOT films exhibiting both mixed and highly face-on orientations, supporting the findings of this study. The authors demonstrated that their enhanced film conductivity could be attributed, at least in part, to a higher face-on orientation and to a lower π-π stacking distance of their PEDOT films. Additionally, they observed that the formation of quinoid structures and the reduction of impurities played a role in modifying film conductivity[49].

HR-TEM and STEM-HAADF coupled to STEM-EDX cross-section measurements of a PEDOT thin film deposited on a silicon substrate at 170 °C (Sample A) were performed. HR-TEM image (**Figure 5a**) reveals the silicon substrate consisting of a crystalline silicon bulk, followed by an amorphous silicon layer and native silicon oxide layer measuring 1-2 nm in thickness. Moreover, on top of this amorphous layer, a second amorphous layer containing heavy elements (revealed by dark contrast) is present. STEM-HAADF image corroborated the presence of this layer (bright contrast in **Figure 5b**) and STEM-EDX mapping (**Figure 5c**) demonstrates that this layer containing Sb and S elements, is typical of PEDOT film composition. From these measurements, the PEDOT thin film thickness was estimated approximately 8±3 nm, in agreement with AFM measurements. Further STEM-EDX mapping measurements were conducted on a larger film section of 1 µm, as depicted in Supplementary Figure S5, showing the conformity and homogeneity of the PEDOT film in terms of both film thickness and chemical composition across the entire analyzed zone. This seems to confirm that the oCVD process operates in a kinetically-limited regime at 170 °C.

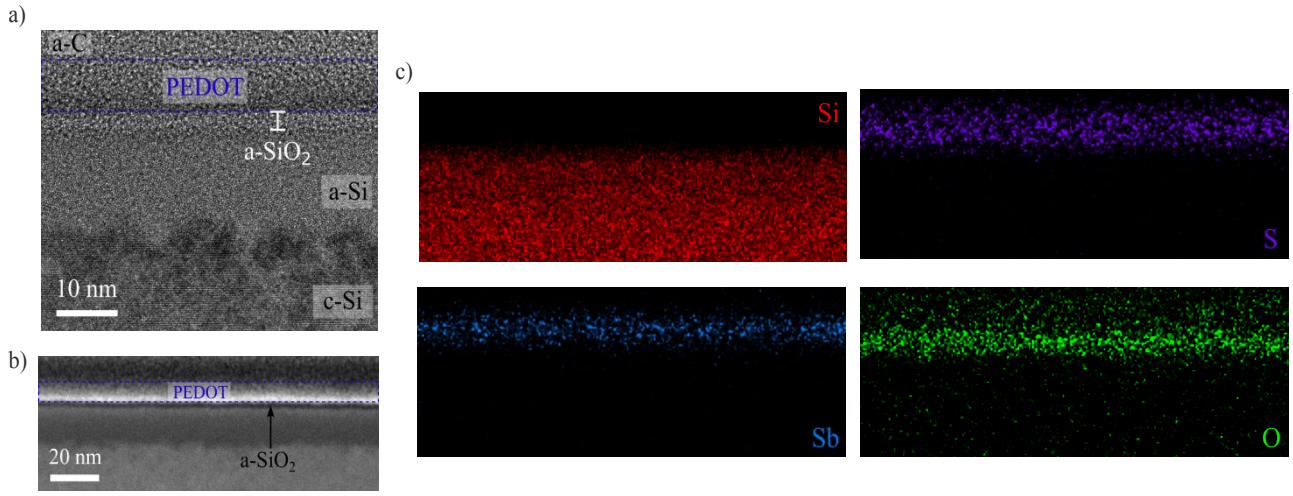

Figure 5. (a) HR-TEM image of the PEDOT thin film deposited on silicon substrate A at 170 °C. **(b)** STEM-HAADF image coupled to **(c)** STEM-EDX mapping for different elements (Si, S, Sb and O).

AFM measurements were performed to extract the root mean square roughness of sample B for the five T_{sub}. The films exhibit relatively low roughness values ranging from 0.56 nm to 1.29 nm with a uniform morphology free of pin-holes, as presented in **Figure 6**. Further details on the roughness values at each temperature are presented in Supplementary Table S4. The obtained values are similar to previous work using the same reagents having a film roughness around 0.71-1.35 nm[43]. This is crucial as OLED devices require a smooth, homogeneous, and uniform surface without pinholes that may generate recombination at the PEDOT interface, which can thus degrade the output device performance. A comparative table summarizing the properties of PEDOT

synthesized using various methods is provided in Supplementary Table S5. This table demonstrates higher maximum values of conductivity and transmittance for PEDOT synthesized by oCVD and oxidative molecular deposition (oMLD) when compared to other methods such as vapor-phase deposition, electrochemical polymerization, and solution-based PEDOT for films of tens of nanometers in thickness. Regardless of the method used to produce PEDOT thin films, smooth surface with low RMS values can be obtained in all cases.

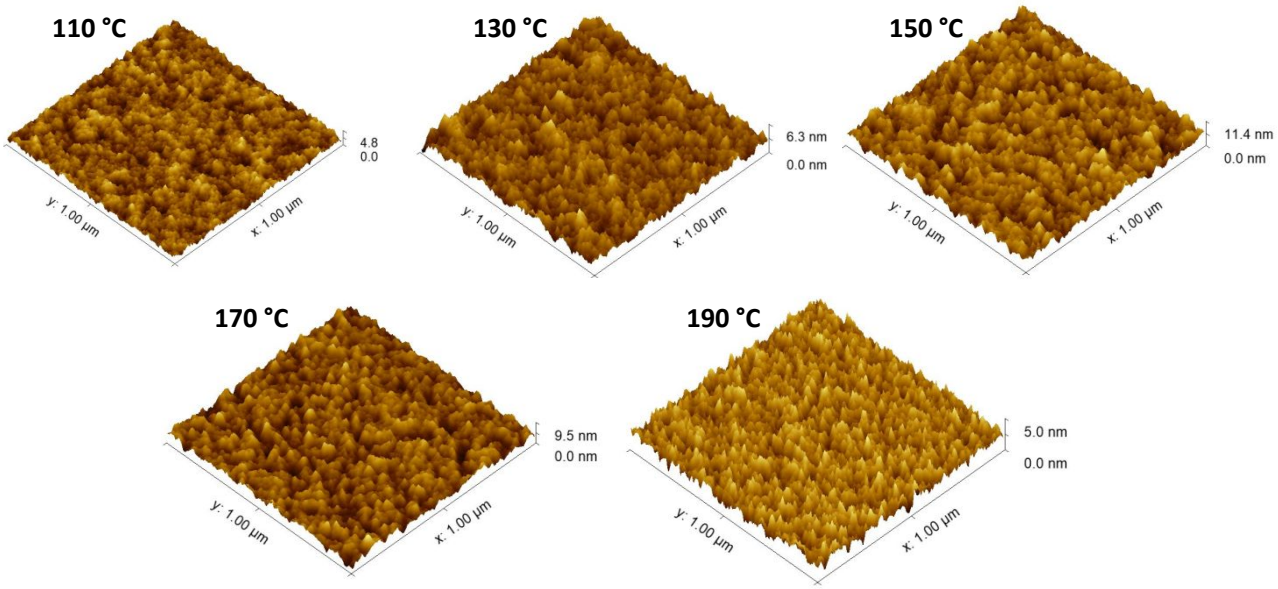

Figure 6. AFM topography images of PEDOT thin films deposited on sample A at different substrate temperatures (from 110 °C to 190 °C).

Furthermore, the roughness values, surface morphology, and chemical bonds are contributing factors to the observed hydrophilic behavior of the samples surface (see Supplementary Table S6 and Figure S6). Indeed, the average contact angle ranges from 54.3° to 44.9° for samples A deposited at 110 °C and 190 °C, respectively. The observed hydrophilic behavior could induce better wetting properties, adhesion, and film formation of the organic layers within the OLED processing and thus performance.

After a thorough investigation into the influence of deposition parameters on the structure, morphology, and properties of oCVD-PEDOT thin films, we successfully achieved high values in terms of both electrical conductivity and transparency. Further, the oCVD PEDOT thin films used for OLEDs were deposited at a temperature of 170 °C with a film thickness of 40-45 nm. These parameters have resulted in the formation of a conformal, homogeneous film with low roughness and high conductivity. This was crucial for achieving a homogeneous emission area in OLEDs, promoting efficient charge generation from PEDOT to the organic emissive layer[58,59]. The PEDOT thin film was successfully integrated as TCE anode for deep blue OLED structures. OLEDs include a cathode of calcium 99.99% (Ca), NPD as both an emissive layer and hole transport layer, and TPBi as both an exciton blocking and electron transport layer (**Figures 7a&b**). For comparison, the OLEDs based on commercial ITO were also fabricated by using similar structure. OLEDs displayed a deep blue light with a maximum of emission centered at 436 nm.

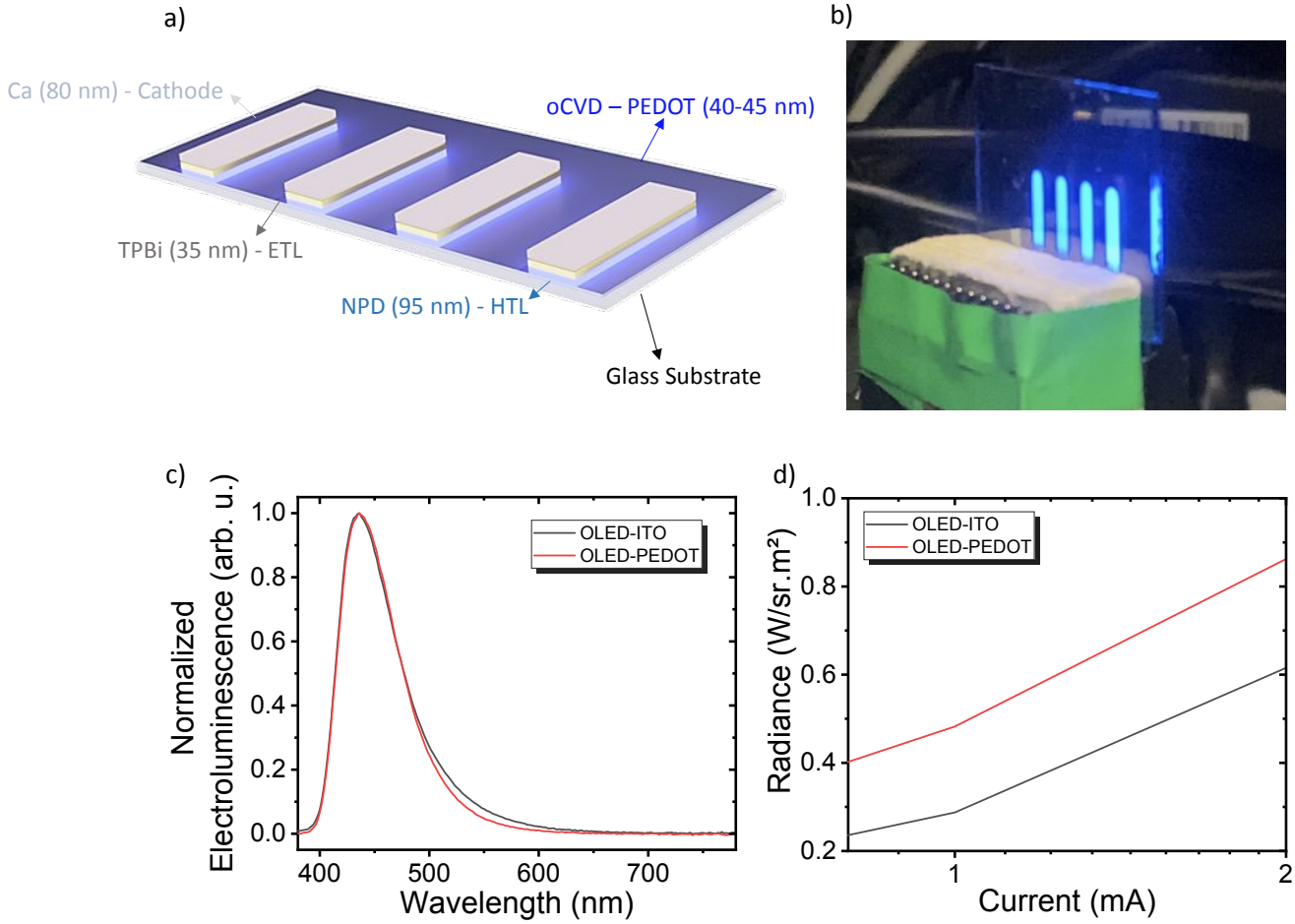

Figure 7. (a) Structure and **(b)** optical image, of four OLED devices comprising a PEDOT thin film by oCVD at 170 ˚C, comparison of the **(c)** electroluminescence spectra, and **(d)** radiance measurements between the reference devices based on an ITO electrode and those with an alternative oCVD-PEDOT thin film-based electrode.

Replacing ITO with oCVD PEDOT in OLEDs resulted in slightly higher performance in terms of radiance and luminance at 2 mA (**Figures 7c&d**). The detailed results are presented in

Table 1, showing an increase of 8.35 Cd/m² and 0.25 W/Sr.m² in luminance and radiance, respectively, compared to the reference device using ITO. The oCVD PEDOT layer demonstrated superior conversion of electrical energy to emitted light, with a higher external quantum efficiency (EQE) of 1.04% at 1 mA, resulting in increased OLED brightness and improved color accuracy. It is worth mentioning that the turn-on voltage of ITO-based and PEDOT-based OLEDs is 3.3 V and 14 V, respectively, for a luminance level of 1 Cd/m^2. This difference can be attributed to the lower conductivity of oCVD-PEDOT compared to ITO, which results in a lower charge diffusion. Still, the oCVD PEDOT layer displayed higher work function of 5.1 - 5.4 eV[60,61] than that of ITO, which was about 4.7 - 5.0 eV[62]. An additional hole injection layer such as PEDOT:PSS is currently used for smoothing ITO surface and to improve hole injection from the ITO anode to the HTL of the OLED. Such HIL are coated from solvent solution and thermal annealing treatment is required in order to effectively remove the residual solvent[14,15]. Due to its high work function (WF) combined with low surface roughness, the oCVD PEDOT thin layers can play the role of both TCE as well as HIL within OLED structure. A comparative table of work functions extracted from the literature for oCVD-PEDOT, solution-based PEDOT, and ITO thin film is presented in Supplementary Table S7. In fact, the Commission Internationale de l'Energie (CIE) coordinates are (0.15, 0.08), as shown in **Figure 8a**. Furthermore, under variation of applied current, the measurements of CIE coordinates show that the chrominance of devices are stable (as shown in **Figure 8b&c**), which would be benefit for applications on displays. These findings are promising as a proof of concept and demonstrate the potential of oCVD PEDOT thin films as solvent-free TCE for ITO-free OLED design. These thin films display high performance, surpassing conventional OLED devices that necessitate the stacking of more than five layers[58,63].

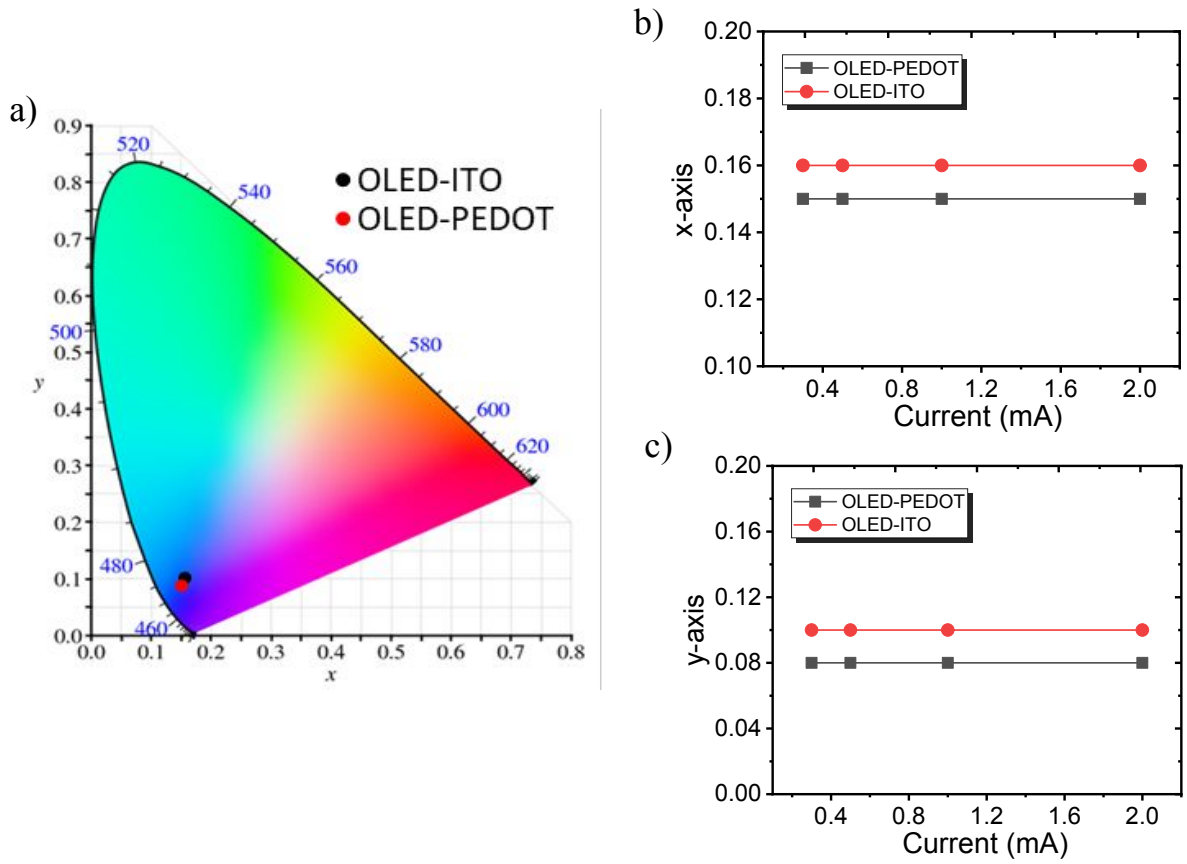

Figure 8. (a). Corresponding emission colors on the CIE 1931 chromaticity diagram. and variation of **(b).** CIE x, and **(c).** CIE y, with current for reference devices based on an ITO electrode and those with an alternative oCVD PEDOT thin film-based electrode.

Table.1 Comparative study of a reference device based on ITO electrodes and an alternative oCVD PEDOT thin film-based device.

Device Structure	Current density ($mA.cm^{-2}$)	Luminance (Cd/m^2)	Radiance ($W/Sr.\ m^2$)	Max Wavelength (nm)	CIE coordinates (x,y)	EQEmax/Current (%, mA)
ITO/NPD (95nm)/TPBi (35nm)/Ca (80nm)	10	63.78	0.61	436	(0.16, 0.10)	0.62/1
PEDOT/NPD (95nm)/TPBi (35nm)/Ca (80nm)		72.13	0.86	436	(0.15, 0.08)	1.04/1

4. CONCLUSION

In summary, this study demonstrates the suitability of the oCVD process for the deposition of PEDOT thin films as an alternative to ITO electrodes in blue OLED devices. Furthermore, this work investigates the effect of substrate temperature on film conductivity and optical transmittance with an increase of both until an optimal value is reached at 170 °C, with a total transmittance of 97% for 8 nm-thick film in the visible range and conductivity exceeding 1600 S/cm. The changes in the film properties of the conjugated polymer were mainly attributed to modifications in the PEDOT molecular structure and chemical composition, as well as the increase in doping level. This was demonstrated through Raman, FTIR, and XPS measurements, which revealed the formation of more quinoid molecular units in the films. The aforementioned factors have contributed significantly to an improved intra-chain charge transport. This was further aligned by studying the film crystallinity using GIXRD and morphology through HRTEM, and AFM, which showed that the PEDOT thin films are semi-crystalline, exhibiting a highly face-on orientation with a smooth surface across different substrate temperatures. This is favorable as it promotes a better percolation pathway and reduces the orientation anisotropy, leading to efficient charge transfer along the PEDOT structure. Additionally, the hydrophilic and smooth surface of oCVD PEDOT is suitable for OLED device fabrication, inducing lower recombination phenomena. A proof of concept of deep blue OLED devices designed on glass substrates using oCVD PEDOT thin films has been successfully demonstrated, resulting in luminance of 72.1 Cd/m² and radiance of 0.86 W/Sr.m² with EQE of 1% and a stable color CIE of (0.15, 0.08). For the sake of comparison, a reference device based on ITO as TCE was also developed, showing that the PEDOT thin film

has slightly higher output performances in terms of luminance and radiance, with an increase of 8.35 Cd/m² and 0.25 W/Sr.m², respectively. In addition, the EQE was increased by a factor of 1.7. This highlights the potential of oCVD PEDOT thin film as a promising alternative to ITO for large-scale OLED devices and more widely for next-generation organic optoelectronic applications.

ASSOCIATED CONTENT

Supporting Information. The Supporting Information is available free of charge at XXXX

AUTHOR INFORMATION

Corresponding Author

Abderrahime Sekkat - LGC, Université de Toulouse, Toulouse INP, CNRS, 31432 Toulouse France ; https://orcid.org/0000-0002-8008-3357 ; Email : abderrahime.sekkat@toulouse-inp.fr

Brigitte Caussat - LGC, Université de Toulouse, Toulouse INP, CNRS, 31432 Toulouse France ; https://www.orcid.org/00000003-4238-2919 ; Email : brigitte.caussat@toulouse-inp.fr

Authors

El Housseiny Houssein - LAPLACE, Université de Toulouse, Toulouse INP, CNRS, UPS, 31062 Toulouse France ; https://www.orcid.org/0009-0007-8295-0462

Diane Samélor - CIRIMAT, Université de Toulouse, Toulouse INP, CNRS, 31030 Toulouse France ;

Benjamin Breig - LGC, Université de Toulouse, Toulouse INP, CNRS, 31432 Toulouse France ;

Eleni Poupaki - LGC, Université de Toulouse, Toulouse INP, CNRS, 31432 Toulouse France ;

Jérôme Esvan - CIRIMAT, Université de Toulouse, Toulouse INP, CNRS, 31432 Toulouse France ;

Olivier Marsan - CIRIMAT, Université de Toulouse, Toulouse INP, CNRS, 31030 Toulouse France ;

Cédric Charvillat - CIRIMAT, Université de Toulouse, Toulouse INP, CNRS, 31030 Toulouse France ;

Alessandro Pugliara - CIRIMAT, Université de Toulouse, Toulouse INP, CNRS, 31030 Toulouse France ; Centre de MicroCaractérisation Raimond Castaing, Université de Toulouse, Toulouse INP, INSA Toulouse, CNRS, 31400 Toulouse, France ; http://orcid.org/0000-0003-1315-1193.

Nicolas Caussé - CIRIMAT, Université de Toulouse, Toulouse INP, CNRS, 31030 Toulouse France ;

Hugues Vergnes - LGC, Université de Toulouse, Toulouse INP, CNRS, 31432 Toulouse France ;

Marc Ternisien - LAPLACE, Université de Toulouse, Toulouse INP, CNRS, UPS, 31062 Toulouse France ;

Cédric Renaud - LAPLACE, Université de Toulouse, Toulouse INP, CNRS, UPS, 31062 Toulouse France ;

Georges Zissis - LAPLACE, Université de Toulouse, Toulouse INP, CNRS, UPS, 31062 Toulouse France ;

Author Contributions

The manuscript was written through contributions of all authors. All authors have given approval to the final version of the manuscript.

Notes

The authors declare no competing financial interest.

ACKNOWLEDGMENT

This work has been partly supported by the pre-maturation POLEN project from the French Occitanie region (ESR_PREMAT-000315). The authors would like to warmly thank Panagiotis Doxas for his contribution in characterizing PEDOT thin films and Claudie Josse of Raimond Castaing Microanalysis Centre for her helpful contribution to the TEM lamella preparation. We would like to thank J. Compain (LGC), E. Prevot (LGC) and D. Sadowski (CIRIMAT) for their help in preparing the experimental setup.

REFERENCES

(1) Hong, G.; Gan, X.; Leonhardt, C.; Zhang, Z.; Seibert, J.; Busch, J. M.; Bräse, S. A Brief

History of OLEDs—Emitter Development and Industry Milestones. *Adv. Mater.* **2021**, *33* (9).

(2) Zou, S. J.; Shen, Y.; Xie, F. M.; Chen, J. De; Li, Y. Q.; Tang, J. X. Recent advances in organic light-emitting diodes: Toward smart lighting and displays. *Mater. Chem. Front.* **2020**, *4* (3), 788–820.

(3) Allemeier, D.; Isenhart, B.; Dahal, E.; Tsuda, Y.; Yoshida, T.; White, M. S. Emergence and control of photonic band structure in stacked OLED microcavities. *Nat. Commun.* **2021**, *12* (1), 1–7.

(4) Baek, S. yeol; Kwak, S. Y.; Kim, S. T.; Hwang, K. Y.; Koo, H.; Son, W. J.; Choi, B.; Kim, S.; Choi, H.; Baik, M. H. Ancillary ligand increases the efficiency of heteroleptic Ir-based triplet emitters in OLED devices. *Nat. Commun.* **2020**, *11* (1), 1–7.

(5) Guo, M.; Ii, J. T. B.; Zhang, H.; Zhao, Y.; Zhao, Y. Challenges and Opportunities of Microelectromechanical Systems for Chemical. *ACS Nano* **2022**, *16* (11), 17778-17801.

(6) Lavric, A.; Petrariu, A. I.; Mutescu, P. M.; Coca, E.; Popa, V. Internet of Things Concept in the Context of the COVID-19 Pandemic: A Multi-Sensor Application Design. *Sensors*

2022, *22* (2).

(7) Daba, H.; Tewodros, N.; Alemneh, B. Device for remote and realtime monitoring of neonatal vital signs in neonatal intensive care unit using internet of things%: proof-of-concept study. *J. Clin. Monit. Comput.* 2022, *37*, 585-592

(8) Papanastasiou, D. T.; Sekkat, A.; Nguyen, V. H.; Jiménez, C.; Muñoz-rojas, D.; Bruckert, F.; Bellet, D. Stable Flexible Transparent Electrodes for Localized Heating of Lab-on-a-Chip Devices. *Adv. Mater. Technol.* 2022, *10* (6), *2200563*..

(9) Ong, G. L.; Ong, T. S.; Yap, S. L.; Liaw, D. J.; Tou, T. Y.; Yap, S. S.; Nee, C. H. A brief review of nanoparticles-doped PEDOT:PSS nanocomposite for OLED and OPV. *Nanotechnol. Rev.* 2022, *11* (1), 1870–1889.

(10) Kang, H. S.; Kim, D. H.; Kim, T. W. Organic light-emitting devices based on conducting polymer treated with benzoic acid. *Sci. Rep.* 2021, *11* (1), 1–9.

(11) Lo, C. C.; Sudheendran Swayamprabha, S.; Hsueh, T. C.; Chavhan, S. D.; Yadav, R. A. K.; Lee, J. R.; Kesavan, K. K.; Chen, S. Z.; Wang, C. W.; Jou, J. H. Modification effect of hole injection layer on efficiency performance of wet-processed blue organic light emitting

diodes. *Org. Electron.* **2021**, *92* (December 2020), 106084.

(12) Cameron, J.; Skabara, P. J. The damaging effects of the acidity in PEDOT:PSS on semiconductor device performance and solutions based on non-acidic alternatives. *Mater. Horizons* **2020**, *7* (7), 1759–1772.

(13) Geng, Q.; Wang, Z.; Gao, Z.; Gao, T.; Li, Y.; Chen, L.; Li, M. Phase Separation to Improve the Conductivity and Work Function of the PEDOT:PSS Solution for Silicon Hybrid Solar Cells. *J. Phys. Chem. C* **2021**, *125* (48), 26379–26388.

(14) Xu, H.; Zhao, X.; Yang, G.; Ji, X.; Zhang, X.; Li, L.; Wu, B.; Ouyang, X.; Ni, Y.; Chen, L.; Hu, H. C. Modification of PEDOT:PSS towards high-efficiency OLED electrode via synergistic effect of carboxy and phenol groups from biomass derivatives. *Chem. Eng. J.* **2022**, *430* (P3), 133014.

(15) Kurosawa, Y.; Murakami, T.; Takahashi, T.; Suzuri, Y. Coverage Performance of PEDOT:PSS Against Particles on a Substrate for OLEDs. *Adv. Mater. Interfaces* **2023**, *10* (5), 1–7.

(16) Zhang, Y.; Liu, K.; Huang, J.; Xia, X.; Cao, J.; Zhao, G.; Fong, P. W. K.; Zhu, Y.; Yan, F.;

Yang, Y.; Lu, X.; Li, G. Graded bulk-heterojunction enables 17% binary organic solar cells via nonhalogenated open air coating. *Nat. Commun.* **2021**, *12* (1), 1–13.

(17) Dijk, G.; Ruigrok, H. J.; O'Connor, R. P. Influence of PEDOT:PSS Coating Thickness on the Performance of Stimulation Electrodes. *Adv. Mater. Interfaces* **2020**, *7* (16), 1–9.

(18) Schultheiss, A.; Sekkat, A.; Nguyen, V. H.; Carella, A.; Benayad, A.; Revaux, A.; Demadrille, R.; Muñoz-Rojas, D.; Simonato, J. P. High performance encapsulation of transparent conductive polymers by spatial atomic layer deposition. *Synth. Met.* **2022**, *284* (November 2021), 1–8.

(19) Luo, S. C.; Yu, H. H.; Wan, A. C. A.; Han, Y.; Ying, J. Y. A general synthesis for PEDOT-coated nonconductive materials and PEDOT hollow particles by aqueous chemical polymerization. *Small* **2008**, *4* (11), 2051–2058.

(20) McFarlane, S. L.; Deore, B. A.; Svenda, N.; Freund, M. S. A one-step, organic-solvent processable synthesis of PEDOT thin films via in situ metastable chemical polymerization. *Macromolecules* **2010**, *43* (24), 10241–10245.

(21) Macher, S.; Schott, M.; Sassi, M.; Facchinetti, I.; Ruffo, R.; Patriarca, G.; Beverina, L.;

Posset, U.; Giffin, G. A.; Löbmann, P. New Roll-to-Roll Processable PEDOT-Based Polymer with Colorless Bleached State for Flexible Electrochromic Devices. *Adv. Funct. Mater.* **2020**, *30* (6).

(22) Yadav, P.; Naqvi, S.; Patra, A. Poly(3,4-ethylenedioxyselenophene): Effect of solvent and electrolyte on electrodeposition, optoelectronic and electrochromic properties. *RSC Adv.* **2020**, *10* (21), 12395–12406.

(23) Jia, Y.; Shen, L.; Liu, J.; Zhou, W.; Du, Y.; Xu, J.; Liu, C.; Zhang, G.; Zhang, Z.; Jiang, F. An efficient PEDOT-coated textile for wearable thermoelectric generators and strain sensors. *J. Mater. Chem. C* **2019**, *7* (12), 3496–3502.

(24) Li, B.; Skorenko, K. H.; Qiu, H.; Mativetsky, J. M.; Dwyer, D. B.; Bernier, W. E.; Jones, W. E. Effects of interfacial modification for vapor phase polymerized PEDOT on glass substrate. *Synth. Met.* **2020**, *260* (September 2019).

(25) Lock, J. P.; Im, S. G.; Gleason, K. K. Oxidative chemical vapor deposition of electrically conducting poly(3,4-ethylenedioxythiophene) films. *Macromolecules* **2006**, *39* (16), 5326–5329.

(26) Gueye, M. N.; Carella, A.; Faure-Vincent, J.; Demadrille, R.; Simonato, J. P. Progress in understanding structure and transport properties of PEDOT-based materials: A critical review. *Prog. Mater. Sci.* **2020**, *108* (November 2019), 100616.

(27) Chelawat, H.; Vaddiraju, S.; Gleason, K. Conformal, conducting poly(3,4-ethylenedioxythiophene) thin films deposited using bromine as the oxidant in a completely dry oxidative chemical vapor deposition process. *Chem. Mater.* **2010**, *22* (9), 2864–2868.

(28) Im, S. G.; Gleason, K. K.; Olivetti, E. A. Doping level and work function control in oxidative chemical vapor deposited poly (3,4-ethylenedioxythiophene). *Appl. Phys. Lett.* **2007**, *90* (15), 88–91.

(29) Viola, W.; Jin, C.; Andrew, T. L. Self-discharge characteristics of vapor deposited polymer electrodes in an all-textile supercapacitor. *Synth. Met.* **2020**, *268* (April), 116483.

(30) Moni, P.; Lau, J.; Mohr, A. C.; Lin, T. C.; Tolbert, S. H.; Dunn, B.; Gleason, K. K. Growth Temperature and Electrochemical Performance in Vapor-Deposited Poly(3,4-ethylenedioxythiophene) Thin Films for High-Rate Electrochemical Energy Storage. *ACS Appl. Energy Mater.* **2018**, *1* (12), 7093–7105.

(31) Wang, X.; Ugur, A.; Goktas, H.; Chen, N.; Wang, M.; Lachman, N.; Kalfon-Cohen, E.; Fang, W.; Wardle, B. L.; Gleason, K. K. Room Temperature Resistive Volatile Organic Compound Sensing Materials Based on a Hybrid Structure of Vertically Aligned Carbon Nanotubes and Conformal oCVD/iCVD Polymer Coatings. *ACS Sensors* **2016**, *1* (4), 374–383.

(32) Bashir, T.; Skrifvars, M.; Persson, N. K. Synthesis of high performance, conductive PEDOT-coated polyester yarns by OCVD technique. *Polym. Adv. Technol.* **2012**, *23* (3), 611–617.

(33) Drewelow, G.; Wook Song, H.; Jiang, Z. T.; Lee, S. Factors controlling conductivity of PEDOT deposited using oxidative chemical vapor deposition. *Appl. Surf. Sci.* **2020**, *501* (June 2019), 144105.

(34) Liu, W.; Li, X.; Li, W.; Ye, Y.; Wang, H.; Su, P.; Yang, W.; Yang, Y. High-performance supercapacitors based on free-standing SiC@PEDOT nanowires with robust cycling stability. *J. Energy Chem.* **2022**, *66*, 30–37.

(35) Bashir, T.; Ali, M.; Cho, S. W.; Persson, N. K.; Skrifvars, M. OCVD polymerization of

PEDOT: Effect of pre-treatment steps on PEDOT-coated conductive fibers and a morphological study of PEDOT distribution on textile yarns. *Polym. Adv. Technol.* **2013**, *24* (2), 210–219.

(36) Smith, P. M.; Su, L.; Gong, W.; Nakamura, N.; Reeja-Jayan, B.; Shen, S. Thermal conductivity of poly(3,4-ethylenedioxythiophene) films engineered by oxidative chemical vapor deposition (oCVD). *RSC Adv.* **2018**, *8* (35), 19348–19352.

(37) Im, S. G.; Olivetti, E. A.; Gleason, K. K. Systematic control of the electrical conductivity of poly (3,4-ethylenedioxythiophene) via oxidative chemical vapor deposition (oCVD). *Surf. Coatings Technol.* **2007**, *201* (22-23 SPEC. ISS.), 9406–9412.

(38) Kim, H.; Zhang, Y.; Rothschild, M.; Roh, K.; Kim, Y.; Jang, H. S.; Min, B. C.; Lee, S. Hybrid Silicon-Polymer Photodetector Engineered Using Oxidative Chemical Vapor Deposition for High-Performance and Bias-Switchable Multi-Functionality. *Adv. Funct. Mater.* **2022**, *32* (29).

(39) Krieg, L.; Meierhofer, F.; Gorny, S.; Leis, S.; Splith, D.; Zhang, Z.; von Wenckstern, H.; Grundmann, M.; Wang, X.; Hartmann, J.; Margenfeld, C.; Manglano Clavero, I.;

Avramescu, A.; Schimpke, T.; Scholz, D.; Lugauer, H. J.; Strassburg, M.; Jungclaus, J.; Bornemann, S.; Spende, H.; Waag, A.; Gleason, K. K.; Voss, T. Toward three-dimensional hybrid inorganic/organic optoelectronics based on GaN/oCVD-PEDOT structures. *Nat. Commun.* **2020**, *11* (1).

(40) Mirabedin, M.; Vergnes, H.; Caussé, N.; Vahlas, C.; Caussat, B. An out of the box vision over oxidative chemical vapor deposition of PEDOT involving sublimed iron trichloride. *Synth. Met.* **2020**, *266* (116419).

(41) Wang, X.; Zhang, X.; Sun, L.; Lee, D.; Lee, S.; Wang, M.; Zhao, J.; Shao-Horn, Y.; Dincă, M.; Palacios, T.; Gleason, K. K. High electrical conductivity and carrier mobility in oCVD PEDOT thin films by engineered crystallization and acid treatment. *Sci. Adv.* **2018**, *4* (9), 1–10.

(42) Wang, X.; Ermez, S.; Goktas, H.; Gradečak, S.; Gleason, K. Room Temperature Sensing Achieved by GaAs Nanowires and oCVD Polymer Coating. *Macromol. Rapid Commun.* **2017**, *38* (12), 1–7.

(43) Kaviani, S.; Mohammadi Ghaleni, M.; Tavakoli, E.; Nejati, S. Electroactive and Conformal

Coatings of Oxidative Chemical Vapor Deposition Polymers for Oxygen Electroreduction. *ACS Appl. Polym. Mater.* **2019**, *1* (3), 552–560.

(44) Muralter, F.; Coclite, A. M.; Lau, K. K. S. Oxidative Chemical Vapor Deposition of Conducting Polymer Films on Nanostructured Surfaces for Piezoresistive Sensor Applications. *Adv. Electron. Mater.* **2021**, *7* (2), 1–5.

(45) Gharahcheshmeh, M. H.; Tavakoli, M. M.; Gleason, E. F.; Robinson, M. T.; Kong, J.; Gleason, K. K. Tuning, optimization, and perovskite solar cell device integration of ultrathin poly(3,4-ethylene dioxythiophene) films via a single-step all-dry process. *Sci. Adv.* **2019**, *5* (11), 1–13.

(46) Dominik, F.; Jones, A. O. F.; Menon, R.; Sariciftci, N. S.; Stadler, P. Metallic conductivity beyond the Mott minimum in PEDOT: Sulphate at low temperatures. *Synth. Met.* **2018**, *240* (November 2017), 59–66.

(47) Atanasov, S. E.; Losego, M. D.; Gong, B.; Sachet, E.; Maria, J. P.; Williams, P. S.; Parsons, G. N. Highly conductive and conformal poly(3,4-ethylenedioxythiophene) (PEDOT) thin films via oxidative molecular layer deposition. *Chem. Mater.* **2014**, *26* (11), 3471–3478.

(48) Im, S. G.; Kusters, D.; Choi, W.; Baxamusa, S. H.; van de Sanden, M. C. M.; Gleason, K. K. Conformal coverage of poly(3,4-ethylenedioxythiophene) films with tunable nanoporosity via oxidative chemical vapor deposition. *ACS Nano* **2008**, *2* (9), 1959–1967.

(49) Heydari Gharahcheshmeh, M.; Robinson, M. T.; Gleason, E. F.; Gleason, K. K. Optimizing the Optoelectronic Properties of Face-On Oriented Poly(3,4-Ethylenedioxythiophene) via Water-Assisted Oxidative Chemical Vapor Deposition. *Adv. Funct. Mater.* **2021**, *31* (14), 1–12.

(50) Mirabedin, M.; Vergnes, H.; Caussé, N.; Vahlas, C.; Caussat, B. Liquid antimony pentachloride as oxidant for robust oxidative chemical vapor deposition of poly(3,4-ethylenedioxythiophene) films. *Appl. Surf. Sci.* **2021**, *554*.

(51) Kim, J. S.; Parsons, G. N. Nanopatterned Area-Selective Vapor Deposition of PEDOT on SiO2vs Si-H: Improved Selectivity Using Chemical Vapor Deposition vs Molecular Layer Deposition. *Chem. Mater.* **2021**, *33* (23), 9221–9230.

(52) Volk, A. A.; Kim, J.-S.; Jamir, J.; Dickey, E. C.; Parsons, G. N. Oxidative molecular layer deposition of PEDOT using volatile antimony(V) chloride oxidant. *J. Vac. Sci. Technol. A*

2021, *39* (3), 032413.

(53) Heydari Gharahcheshmeh, M.; Gleason, K. K. Texture and nanostructural engineering of conjugated conducting and semiconducting polymers. *Mater. Today Adv.* **2020**, *8*, 100086.

(54) *Safety Data Sheet Antimony(V) chloride*. https://www.sigmaaldrich.com/FR/fr/product/aldrich/215171.

(55) King, Z. A.; Shaw, C. M.; Spanninga, S. A.; Martin, D. C. Structural, chemical and electrochemical characterization of poly(3,4-Ethylenedioxythiophene) (PEDOT) prepared with various counter-ions and heat treatments. *Polymer (Guildf).* **2011**, *52* (5), 1302–1308.

(56) Kim, D.; Zozoulenko, I. Why Is Pristine PEDOT Oxidized to 33%? A Density Functional Theory Study of Oxidative Polymerization Mechanism. *J. Phys. Chem. B* **2019**, *123* (24), 5160–5167.

(57) Kirchmeyer, S.; Reuter, K. Scientific importance, properties and growing applications of poly(3,4-ethylenedioxythiophene). *J. Mater. Chem.* **2005**, *15* (21), 2077–2088.

(58) Lee, S. M.; Kwon, J. H.; Kwon, S.; Choi, K. C. A Review of Flexible OLEDs Toward

Highly Durable Unusual Displays. *IEEE Trans. Electron Devices* **2017**, *64* (5), 1922–1931.

(59) Lee, S.; Han, J. H.; Lee, S. H.; Baek, G. H.; Park, J. S. Review of Organic/Inorganic Thin Film Encapsulation by Atomic Layer Deposition for a Flexible OLED Display. *Jom* **2019**, *71* (1), 197–211.

(60) Barr, M. C.; Carbonera, C.; Po, R.; Bulović, V.; Gleason, K. K. Cathode buffer layers based on vacuum and solution deposited poly(3,4-ethylenedioxythiophene) for efficient inverted organic solar cells. *Appl. Phys. Lett.* **2012**, *100* (18).

(61) Im, S. G.; Gleason, K. K.; Olivetti, E. A. Doping level and work function control in oxidative chemical vapor deposited poly (3,4-ethylenedioxythiophene). *Appl. Phys. Lett.* **2007**, *90* (15).

(62) Park, Y.; Choong, V.; Gao, Y.; Hsieh, B. R.; Tang, C. W. Work function of indium tin oxide transparent conductor measured by photoelectron spectroscopy. *Appl. Phys. Lett.* **1996**, *68* (19), 2699–2701.

(63) Yan, M.; Zhang, Q.; Zhao, Y.; Yang, J.; Yang, T.; Zhang, J.; Li, X. Applications of transparent conducting oxides in organic light emitting devices. *J. Nanosci. Nanotechnol.*

2015, *15* (9), 6279–6294.

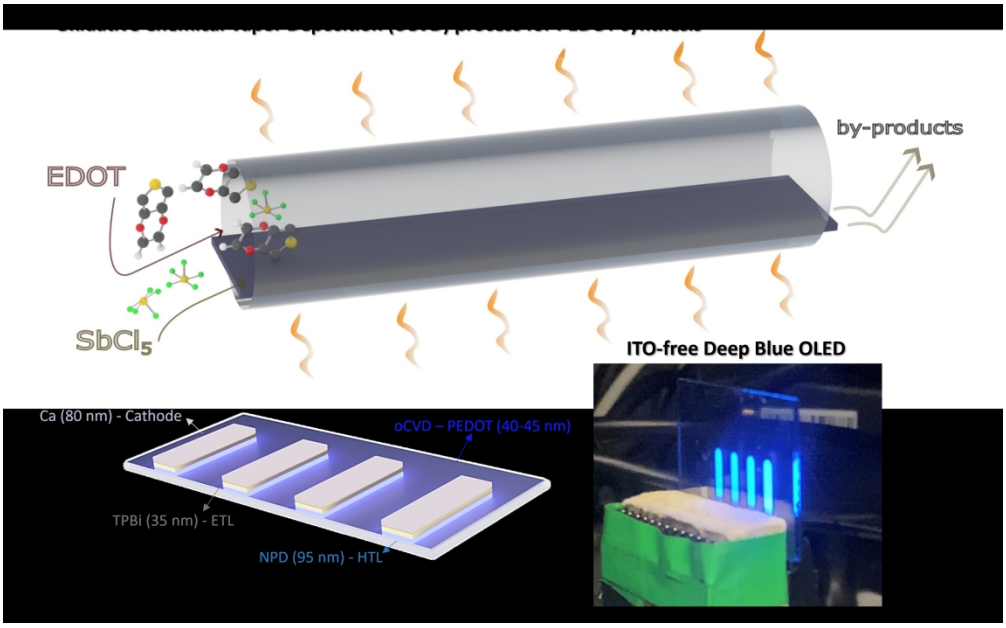

Oxidative chemical vapor deposition (oCVD) process for PEDOT synthesis in ITO-free deep blue OLEDs

297x184mm (300 x 300 DPI)